# Pressure-induced Anderson-Mott Transition in Elemental Tellurium

## Supplementary Material

*Jaime F. Oliveira, Magda B. Fontes, Marcus Moutinho, Stephen E. Rowley, Elisa Baggio-Saitovitch, Marcello B. Silva Neto, and Carsten Enderlein*

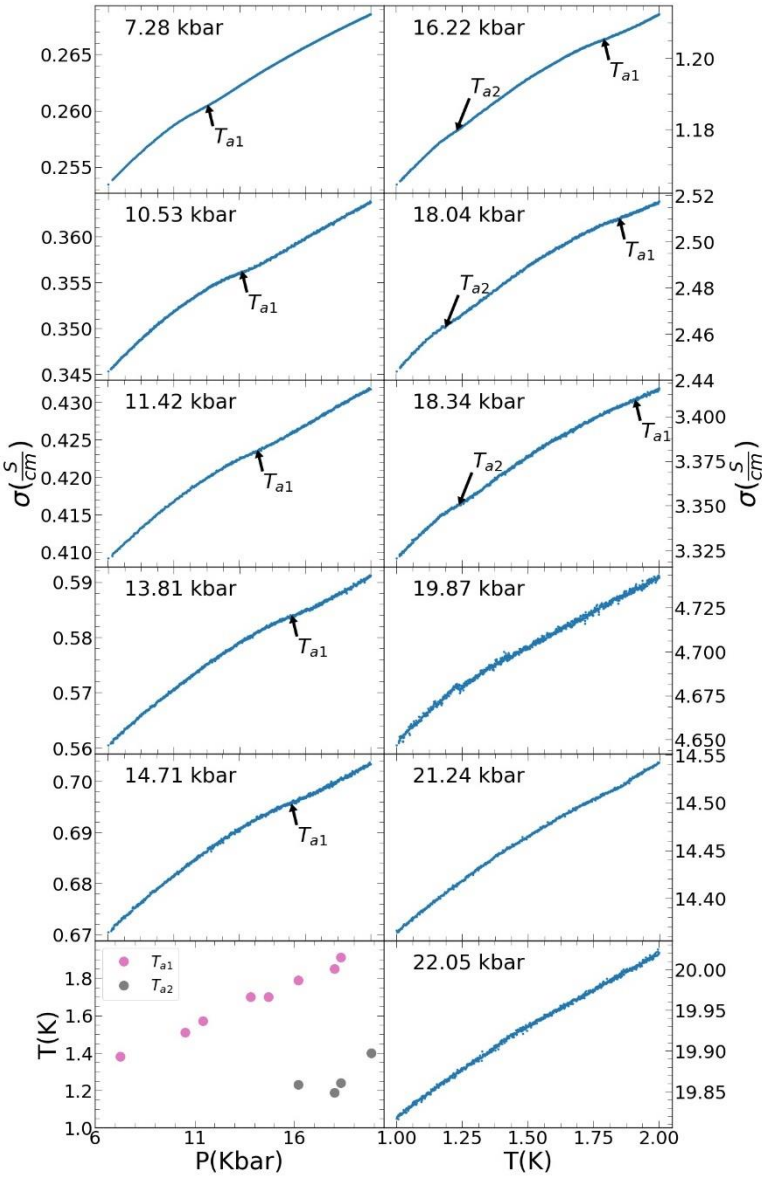


*Supplementary Figure 1 - ρ(T ) curves to display the anomalies. $T_{a1}$ and $T_{a2}$ refer to the first and the second anomaly, respectively. The first one, we associate with the entrance of the chemical potential into the valence band. The second one, we associate with the mobility edge. The exact nominal positions, which are marked by arrows, have been determined by taking the peak position of the maximum in the first derivative.*

## Supplementary Note 1: DFT calculations

For the specific calculations, giving the results in Fig. 3 in the paper, we relax the tellurium hexagonal Bravais-lattice structure without the spin-orbit coupling (SOC), varying the target

pressure from -20 kbar to the +20 kbar. For each step of 5 kbar, we extract the in-plane and out-of-plane lattice parameters, *a* and *c*, respectively, as well as the internal atomic position parameter *u*, as shown in Fig. 3 a), (with $|\boldsymbol{a}_1| = |\boldsymbol{a}_2| = a$). After that, we included the SOC in a self-consistent calculation for each set of geometric parameters, to compute the valence band structures (Figs. 3 **g**-**i**) and the two-dimensional spin texture (Figs. 3 **d**-**f**). We see that a equivalent pressure of -20 kbar reproduces the well know "camel-back-shape" (CBS) of the valence band (VB) structure along of the the K-H-K direction of the Brillouin zone, as shown in Fig. 3 **g**, with a local minimum at the H point (see Fig. 3 **c** for the special points and reciprocal lattice vectors). On the other hand, for a pressure of +10 kbar, the CBS vanishes, and the VB assumes a "dromedary-like shape" (DLS), as one can see in Fig. 3 **i**.

The geometric parameters for each pressure are listed in Table 1. Figs. 3**d**-**f** show the two-dimensional contour plot of the VB along of the $k_x \times k_z$ reciprocal area close to the H point. The white arrows represent the projection of the spins in the plane and the black curve is an equi-energy contour for each pressure which keeps the electronic density $n = \frac{1}{VN_k}\sum_k \left[\exp\left(\frac{\varepsilon_k}{k_B T}\right) + 1\right]^{-1}$ approximately constant at $10^{16}$ cm$^{-3}$. In this expression $V$ is the unit cell volume, $N_k$ is the total amount of k-points in the BZ while the chemical potential is set to zero at room temperature in the Fermi weight. We used the small local minimum located at -2.0 meV for -5 kbar as a reference to compute the density for the other pressures.

**Geometric parameters for each pressure obtained without the spin-orbit coupling**

| *P/kbar* | *a/Å* | *c/a* | *u/a* | *ΔE/meV* |
|---|---|---|---|---|
| *-20* | 4.76725 | 1.24466 | 0.244616 | -1.0 |
| *-5* | 4.54050 | 1.30258 | 0.265988 | -2.0 |
| *10* | 4.43664 | 1.32579 | 0.279711 | -7.0 |

The same parameters are used to compute the band structure and the spin texture with spin-orbit coupling. ΔE is an equi-energy level which keeps the electronic density constant at $10^{16}$ cm$^{-3}$.

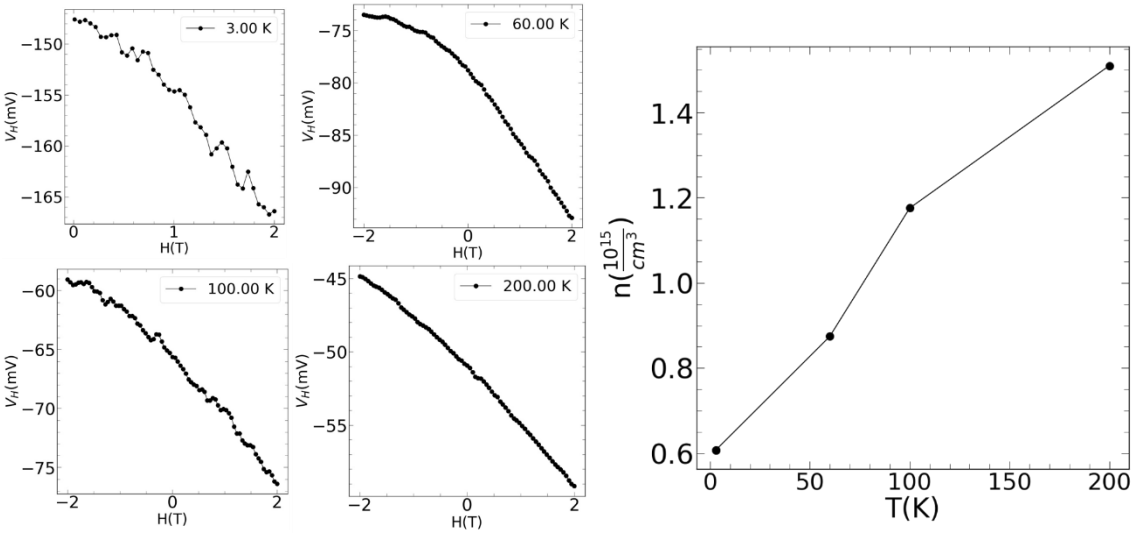


*Supplementary Figure 2 – The four left panels display the Hall effect measurements at four different temperatures. On the right, we see the derived charge densities vs Temperature. As mentioned in the paper, we do not necessarily assume that the derived charge carrier densities really reflect the physics of the system.*

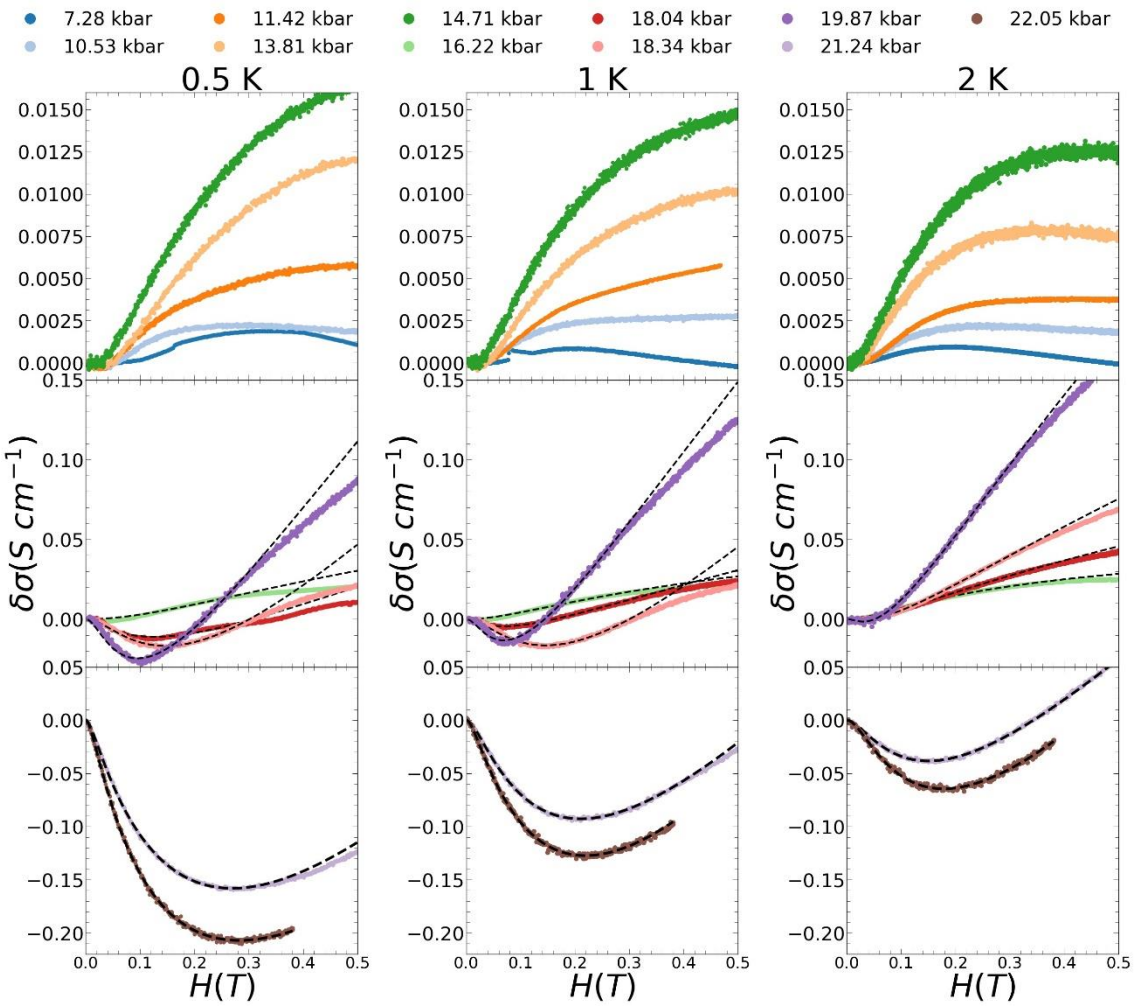


*Supplementary Figure 3 - Magnetoconductance measurements for all pressures for 0.5K, 1K and 2K. with respective fits using the magnetoconductance formula from the paper for P > 16 kbar .*

## Supplementary Note 2: Quantum corrections to magnetoconductance

The exact fitting function is

$$\delta\sigma = A \cdot \frac{e^2}{\hbar} \cdot \frac{1}{2\pi^2} \cdot \sqrt{\frac{e \cdot H}{\hbar}} \cdot \left\{ \frac{3}{2} f_3\left(\frac{H}{H_{s.o.}}\right) + f_3\left(\frac{H}{H_v}\right) + \frac{1}{2} f_3\left(\frac{H}{H_\gamma}\right) - \frac{1}{2} f_3\left(\frac{H}{H_\varphi}\right) \right\}.$$

The strong correlations among the fitting parameters for the metallic phase, lead to extremely high errors (speaking only of the error resulting from the fit. This does not include the errors from experimental set up). Those values with a comparably small error, show pressure dependencies, as demonstrated in Supplementary Fig.4.

For the pressure point at 22.05 kbar, we took measurements at more temperatures to check, if we get the linear temperature dependence of the dephasing field from thermal phonons (see Supplementary Fig. 5).

In the insulating phase, for low fields, the MR can be roughly approximated by a parabola,

$$\delta\sigma \approx C + BH^2.$$

However, specifically for extremely low fields and low temperatures, this fit is challenging, due to the interfering weak antilocalization.

### Supplementary Table 1: Fitting parameters at 0.5 K

| P (Kbar) | A | $H_{S.O.}(T)$ | $H_v(T)$ | $H_\gamma(T)$ | $H_\varphi(T)$ | Error A | Error $H_{S.O.}$ (T) | Error $H_v$ (T) | Error $H_\gamma$ (T) | Error $H_\varphi$ (T) |
|---|---|---|---|---|---|---|---|---|---|---|
| 16.22 | 1.0076 | 330.1911 | 15.9359 | 0.120736 | 0.14846 | 0.001008 | 33.01911 | 1.59359 | 0.012074 | 0.014846 |
| 18.03 | 0.1934 | 175482.8 | 0.040847 | 56258241 | 0.010193 | 7.54E-05 | 1249430 | 0.000922 | 64917685 | 0.000505 |
| 18.34 | 0.6065 | 47912.32 | 0.065725 | 640843.9 | 0.024369 | 0.000121 | 115576.5 | 0.000682 | 1358948 | 0.000421 |
| 19.86 | 0.647 | 137798.1 | 0.03446 | 1854321 | 0.01015 | 0.000104 | 442296.3 | 0.000462 | 4892812 | 0.000246 |
| 21.24 | 0.6007 | 0.107782 | 53444.7 | 636619.2 | 0.004331 | 4.05E-05 | 0.000236 | 366414.6 | 2663860 | 5.74E-05 |
| 22.05 | 0.8722 | 12195.22 | 0.065543 | 33.48843 | 0.004496 | 0.000377 | 134183.6 | 0.002589 | 6553.983 | 0.000281 |

### Supplementary Table 2: Fitting parameters at 1 K

| P (Kbar) | A | $H_{S.O.}(T)$ | $H_v(T)$ | $H_\gamma(T)$ | $H_\varphi(T)$ | Error $H_{S.O.}$ (T) | Error $H_v$ (T) | Error $H_\gamma$ (T) | Error $H_\varphi$ (T) | Error $H_{S.O.}$ (T) |
|---|---|---|---|---|---|---|---|---|---|---|
| 16.22 | 0.0289 | 0.034651 | 806.3025 | 2018.274 | 0.111026 | 0.00047 | 0.021177 | 285117 | 952743.2 | 0.865041 |
| 18.03 | 0.1231 | 378.7047 | 0.023949 | 27310222 | 0.006603 | 1.23E-05 | 23787.02 | 0.000252 | 19764168 | 0.000128 |
| 18.34 | 0.5719 | 43646.51 | 0.063907 | 27591.96 | 0.023338 | 0.000112 | 117223.8 | 0.000667 | 288503.3 | 0.000408 |
| 19.86 | 0.62 | 250197.9 | 0.02935 | 2238939 | 0.010418 | 9.48E-05 | 673847.8 | 0.000474 | 6550126 | 0.000268 |
| 21.24 | 0.561 | 0.091082 | 33094.65 | 8111.339 | 0.007256 | 0.000112 | 0.000327 | 511983 | 488052.5 | 0.000222 |
| 22.05 | 0.6819 | 0.459255 | 0.067576 | 862.0285 | 0.005747 | 0.000646 | 0.154318 | 0.006116 | 153021.6 | 0.000659 |

### Supplementary Table 3: Fitting parameters at 2K

| P (Kbar) | A | $H_{S.O.}(T)$ | $H_v(T)$ | $H_\gamma(T)$ | $H_\varphi(T)$ | Error $H_{S.O.}$ (T) | Error $H_v$ (T) | Error $H_\gamma$ (T) | Error $H_\varphi$ (T) | Error $H_{S.O.}$ (T) |
|---|---|---|---|---|---|---|---|---|---|---|
| 16.22 | 0.5322 | 18.32619 | 20.32196 | 0.035218 | 0.046047 | 0.000532 | 1.832619 | 2.032196 | 0.003522 | 0.004605 |
| 18.03 | 0.0967 | 1388126 | 0.012874 | 214885.8 | 0.006281 | 5.59E-06 | 1173962 | 0.000209 | 1526475 | 0.000169 |
| 18.34 | 0.2229 | 42075.29 | 0.026532 | 37756.94 | 0.014647 | 1.52E-05 | 121423.8 | 0.000315 | 352933.1 | 0.000248 |
| 19.86 | 0.5243 | 147852.5 | 0.023708 | 2271684 | 0.012028 | 5.92E-05 | 417685.2 | 0.000466 | 5242585 | 0.000346 |
| 21.24 | 0.4474 | 0.074423 | 23078.26 | 39764.43 | 0.010571 | 0.000105 | 0.00071 | 428481.9 | 1271818 | 0.000316 |
| 22.05 | 0.7518 | 0.853306 | 0.058076 | 280.3354 | 0.011909 | 0.000732 | 0.330114 | 0.001181 | 80380.19 | 0.000919 |

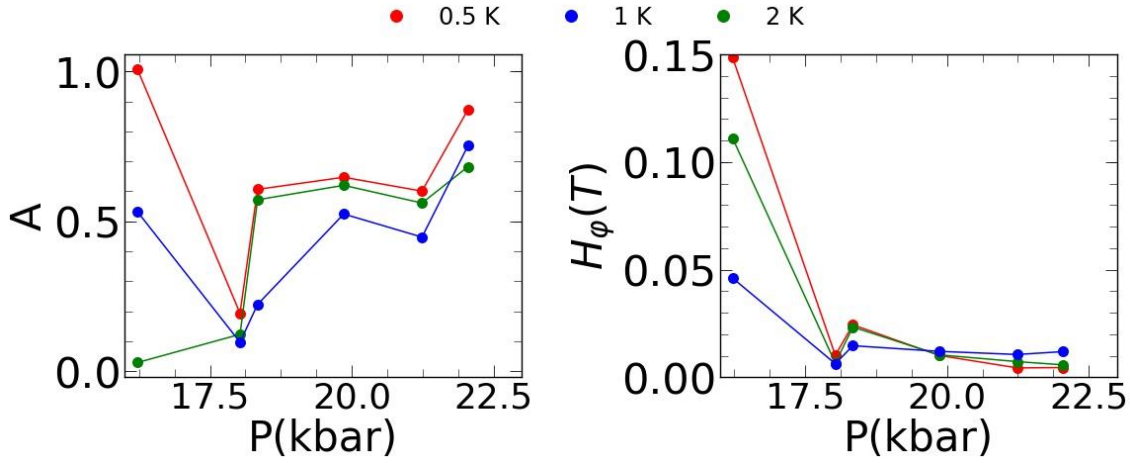


*Supplementary Figure 4 – Development of the pre-factor A, the characteristic spin orbit field and the characteristic dephasing field.*

## Supplementary Table 4: Fitting parameters at 22.05 kbar

| T (K) | A | $H_{S.O.}(T)$ | $H_{\nu}(T)$ | $H_{\gamma}(T)$ | $H_{\varphi}(T)$ | Error A | Error $H_{S.O.}(T)$ | Error $H_{\nu}(T)$ | Error $H_{\gamma}(T)$ | Error $H_{\varphi}(T)$ |
|---|---|---|---|---|---|---|---|---|---|---|
| 0.5 | 0.7326 | 0.10684 | 52.48894 | 2126.425 | 0.003562 | 0.000138 | 0.003466 | 10965.87 | 200456.6 | 0.000116 |
| 0.6 | 0.6904 | 0.10275 | 11.01456 | 845626.5 | 0.003851 | 0.000233 | 0.005683 | 398.2372 | 6123040 | 0.000208 |
| 0.7 | 0.6599 | 0.097835 | 21.05121 | 571.0596 | 0.004006 | 0.000211 | 0.004391 | 1711.824 | 137529.2 | 0.000201 |
| 0.9 | 0.622 | 0.092312 | 106747 | 52018.95 | 0.004927 | 7.92E-05 | 0.000232 | 920522.5 | 1238588 | 0.000115 |
| 1 | 0.6436 | 0.091001 | 12.72411 | 4007.918 | 0.005475 | 0.000269 | 0.003828 | 518.5955 | 333735.3 | 0.000295 |
| 1.5 | 0.5249 | 0.081188 | 70.95417 | 80.77332 | 0.005999 | 0.000217 | 0.00227 | 26696.63 | 54292.78 | 0.000314 |
| 2 | 0.5243 | 0.08953 | 0.671814 | 0.669318 | 0.009223 | 0.000798 | 0.015401 | 2553.337 | 5081.159 | 0.001228 |

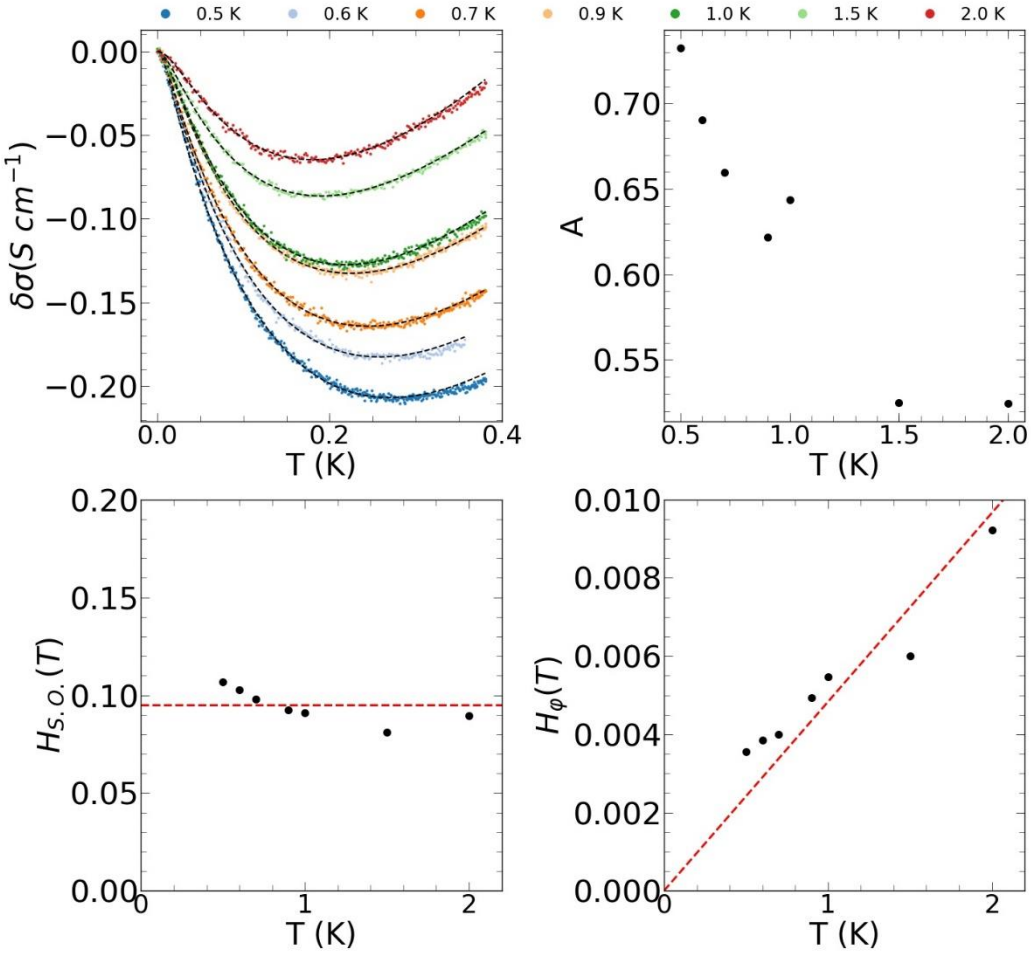


*Supplementary Figure 5 - Magnetoconductance measurements at 22.05 for different temperatures with the A, $H_{S.O.}$ and $H_{\varphi}$ fit parameters. One can see that the function fits the magnetoconductance data very well. $H_{\varphi}$ goes linearly to zero with the temperature, as one would expect and the spin orbit relaxation field $H_{s.o.}$ remains constant. The pre-factor A seemingly diverges when approaching 0K, which is qualitatively consistent with the fact that the number of conduction channels in the the metallic phase should increase approaching zero Kelvin.*

**Supplementary Table 5: Fitting parameters at 0.5 K**

| *P (kbar)* | *B ($S/T^2cm$)* | *C (mS/cm)* |
|---|---|---|
| *7.28* | 2.671 | -0.25 |
| *10.53* | 13.4698 | -0.37 |
| *11.42* | 19.6266 | -0.25 |
| *13.81* | 25.9366 | -0.53 |
| *14.71* | 48.5061 | -0.7 |

**Supplementary Table 6: Fitting parameters at 1 K**

| *P (kbar)* | *B ($S/T^2cm$)* | *C (mS/cm)* |
|---|---|---|
| *7.28* | 8.0516 | -3.99E-05 |
| *10.53* | 18.2538 | -5.50E-05 |
| *11.42* | 17.9198 | -0.00011 |
| *13.81* | 49.5805 | -0.0001 |
| *14.71* | 91.234 | -0.0002 |

**Supplementary Table 7: Fitting parameters at 2 K**

| *P* | *B ($S/T^2cm$)* | *C (mS/cm)* |
|---|---|---|
| *7.28* | 8.0516 | -0.00026 |
| *10.53* | 18.2538 | -0.00056 |
| *11.42* | 17.9198 | -0.00024 |
| *13.81* | 49.5805 | -0.00139 |
| *14.71* | 91.234 | -0.00045 |

## Supplementary Note 3: Discussion of possible alternative origins of the conductivity saturation at low temperatures

In the paper, we explain how spin orbit coupling leads naturally to a finite conductivity at zero Kelvin. Our results are consistent with the experimental data and $\delta\sigma$ demonstrates critical behaviour, as one would expect, if the saturation originates from the spin orbit coupling. However, a saturation of a physical constant in the mK range is often interpreted in different ways. Therefore, we want to discuss potential other explanations here and explain, why we can exclude them.

### Cooling / self-heating problems

Sample self-heating or other thermal transfer problems can lead to response functions, which seemingly flatten in the lowest temperature range. To exclude this as the origin for the observed resistivity saturation, we repeated the measurement first with different current densities and thereafter, again, after warming up the system, tightening all thermal contacts and we received exactly the same resistivity curves.

### Possible surface state

Saturation of physical quantities at very low temperatures are often interpreted in terms of possible surface states. There are many reasons, why such an interpretation in our case does not to seem adequate. One of them would be the surprising change of mobility upon the application of pressure, which would manifest itself in the change of saturation conductivity value. However, we can make a more quantitative argument:

The conductivity measured is around $0.02\ \mathrm{S}$. With a sample length of $3\ \mathrm{mm}$ and a sample wideness of about $1\ \mathrm{mm}$. If we assume that the conduction happens via the surface, this would lead to a surface conductivity of very roughly (we are interested in order of magnitudes) $\sigma = 0.01\ \mathrm{S}$. We might assume a rough charge carrier density of $n = 10^{12}\ \mathrm{cm}^{-2}$, as it is known from metallic surface states. Now, the electrical conductivity satisfies

$$\sigma = ne\mu,$$

With $\mu$ being the mobility. This leads to a mobility of roughly $60000\,\frac{\mathrm{cm}^2}{\mathrm{V\,s}}$, which would be a very impressive, but not very likely result for the untreated surface of a brittle and relatively soft material.

## Supplementary Note 4: Delocalization due to spin-orbit interaction

When all electrons are localized, their wavefunctions fade away within distances of the order of the localization length, $\xi_L$. In this case, the sample size dependent conductance $g(L)$ at $T = 0$ is due to the exponential tails of the wavefunctions and $g(L) = g_c e^{-L/\xi_L}$. This is simply the integral solution to the renormalization group equation associated to the $\beta$-function $\beta(g) = \frac{\mathrm{d}\ln g}{\mathrm{d}\ln L} = \ln(g/g_c)$, which is negative below the critical conductance $g = g_c$, indicating insulating behaviour. The temperature dependence of the conductance is obtained by replacing $L$ with some inelastic dephasing length $L_\varphi(T) = \sqrt{D\tau_\varphi(T)}$, which should be the inelastic dephasing channel relevant to the conduction mechanism. In this case, $g(T) = g_0 e^{-L_\varphi(T)/\xi_L}$.

Typically, the inelastic dephasing time is calculated from the inverse transition rate to neighbouring sites, $\tau_\varphi \sim \Gamma^{-1}$. Such average transition rate may, in turn, be calculated in a straightforward manner using Fermi's golden rule $\Gamma \sim \int \mathrm{d}R R^2 \int \mathrm{d}(\Delta\varepsilon)|M|^2 \exp\left(-\frac{2R}{\xi_L} - \frac{\Delta\varepsilon}{k_B T}\right)$, where $M$ is the pre-exponential factor for the transition rate. In the regime of weak localization, if the phase coherence is destroyed by hops over *optimal hopping* distances, $R \sim \bar{r}$, that are usually accompanied by large energy variations, $\Delta\varepsilon \gg k_B T$, then, when calculating $\Gamma$, one must include Mott's constraint connecting $R$ to the density of states, $N(\varepsilon)$, such that $\bar{r}^d N(\varepsilon_F) \sim$const. In this case one obtains $L_\varphi \sim T^{-b}$, with $b = 1/(d+1)$, or, equivalently, Mott's variable range hopping law $g(L) = g_c \exp\{-(T_0/T)^{1/(d+1)}\}$, with $T_0 \sim 1/N(\varepsilon_F)\xi_L^d$.

If however the phase coherence is destroyed by *non-optimal hops*, $R \sim L_{s.o.}$, within a thin layer of thickness $\Delta\varepsilon \sim k_B T$ near the Fermi level, then one concludes that $L_\varphi \sim L_{s.o.} = \sqrt{D\tau_{s.o.}}$. The spin-orbit scattering does not depend on the temperature. As a result, we end up with an expression for the hopping conductance $g(T) = g_0^{s.o.} \exp\{L_{s.o.}/\xi_L\}$, which, for the case when the spin-orbit length diverges with the localization length, $L_{s.o.} \sim \xi_L$, shows saturation at the lowest temperatures $g(T \to 0) \neq 0$.

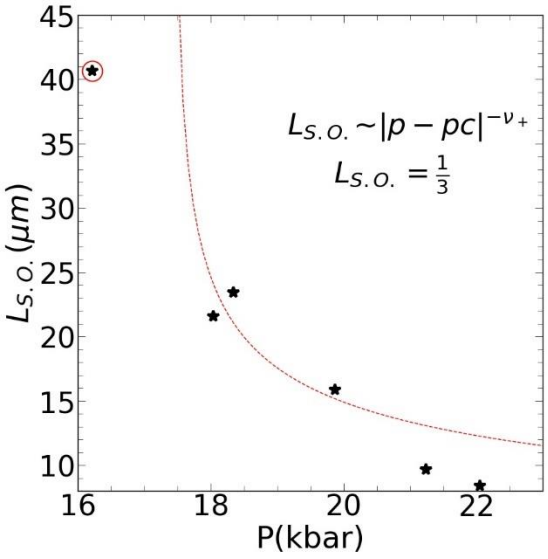


*Figure 6: The divergence of the spin orbit relaxation length when approaching the quantum critical point from the metallic side*

## Supplementary Note 5: Quantum corrections in the disordered metallic phase

Let $1/\tau$ represent the frequency associated to elastic scattering events, those where the temporal variation of the wave-function is unchanged, and let $1/\tau_\varphi$ represent the frequency associated to inelastic (dephasing) scattering events, those where the electron loses memory of its phase prior to the collision. In this case, the relative corrections to conductivity due to the quantum interference among the different possible diffusion paths in a system with spin-orbit interaction is given by Vollhardt and Woelfle (PRL, 1982, **48**, 10, pp. 699-702),

$$\frac{\delta\sigma}{\sigma} \sim -\int_{\tau}^{\tau_\varphi} \mathrm{d}t \frac{v_F \lambda^{d-1}}{a^{3-d}(Dt)^{\frac{d}{2}}} \left(\frac{3}{2} e^{-\frac{t}{\tau_{s.o.}}} - \frac{1}{2}\right),$$

with $v_F$ being the Fermi velocity, $\lambda$ the de Broglie wavelength, $a$ the film thickness or wire diameter (for the cases $d = 2{,}1$ respectively), $d = 3$ for bulk systems, and with $D$ being the diffusion constant. Typically, the inelastic dephasing time is temperature dependent, $\tau_\varphi \propto T^{-p}$, while the spin-orbit relaxation time, $\tau_{s.o.}$, is not. Thus, at sufficiently high temperatures, when $\tau_\varphi \ll \tau_{s.o.}$, we can neglect the spin-orbit interaction, $\tau_{s.o.} \to \infty$, approximate $e^{-t/\tau_{s.o.}} \sim 1$, and integrate over time. For $d = 3$ one obtains $\sigma \sim \frac{e^2}{\hbar} L_\varphi^{-1} + \text{const.}$, where the inelastic dephasing length is $L_\varphi = \sqrt{D\tau_\varphi}$. If the dephasing mechanism is via electron-electron scattering, where $p = 1$ and $\tau_\varphi = \hbar/T$, we end up with the observed law $\sigma(T) = \sigma_0 + m\sqrt{T}$, with $m = \frac{e^2}{\hbar}\frac{1}{\sqrt{D\hbar}}$. The precise expression for $\sigma_0$, however, depends whether one is below or beyond the Ioffe-Regel limit, $k_F l = 1$, where $l$ is the electronic mean free path. Near criticality, $k_F l < 1$, one arrives at $\sigma_0 = \frac{e^2}{\hbar}\xi^{-1}$, where $\xi$ is the correlation length, while deep inside the diffusive regime, $k_F l > 1$, one recovers the Drude diffusive conductivity formula, $\sigma_0 = \frac{e^2}{\hbar}\frac{(k_F l)^2}{l}$, in such a way that, precisely at $k_F l = 1$ and $\xi = l$ the two expressions coincide (see also V. F. Ghantmakher, in *Electrons and disorder in solids*, International series of monographs on physics, Clarendon Press, Oxford (2005)).